

Engineering carbon chains from mechanically stretched graphene-based materials

E. Erdogan,^{1,*} I. Popov,² C. G. Rocha,³ G. Cuniberti,^{3,4} S. Roche,^{3,5,6} and G. Seifert¹

¹*Institut für Physikalische Chemie, Technische Universität Dresden, D-01062 Dresden, Germany*

²*School of Physics and CRANN, Trinity College, Dublin 2, Ireland*

³*Institute for Materials Science and Max Bergmann Center of Biomaterials, Dresden University of Technology, D-01062 Dresden, Germany*

⁴*Division of IT Convergence Engineering, POSTECH, Pohang 790-784, Republic of Korea*

⁵*Centre d' Investigació en Nanociència i Nanotecnologia (ICN-CSIC), UAB Campus, E-08193 Bellaterra, Spain*

⁶*Institució Catalana de Recerca i Estudis Avançats (ICREA), E-08100 Barcelona, Spain*

(Received 26 October 2010; published 4 January 2011)

The electrical response of graphene-based materials can be tailored under mechanical stress. We report different switching behaviors that take place in mechanically deformed graphene nanoribbons prior to the breakage of the junction. By performing tight-binding molecular dynamics, the study of structural changes of graphene nanoribbons with different widths is achieved, revealing that carbon chains are the ultimate bridges before the junction breaks. The electronic and transport calculations show that binary ON/OFF states can be switched prior to and during breakage depending on the atomic details of the nanoribbon. This work supports the interpretation of recent experiments on nonvolatile memory element engineering based on graphene break junctions.

DOI: [10.1103/PhysRevB.83.041401](https://doi.org/10.1103/PhysRevB.83.041401)

PACS number(s): 61.46.Km, 73.63.-b, 62.25.-g

Current advanced etching techniques involving chemical, mechanical, or irradiation processes have enabled the experimental realization of unique sp^2 -carbon-based nanostructures with considerably high atomic resolution.^{1,2} As prominent members of such sp^2 -carbon family, carbon nanotubes³ and graphene-based materials^{4,5} deserve special attention from the scientific community because of their versatile electronic (and transport) properties. Such materials have paved the way for studies focusing on the designing of ultimate nanoscale devices, for instance, field-effect transistors,⁶ flexible electronic displays,⁷ and nanoelectromechanical systems (NEMS) working as mechanical sensors.⁸ Recent experimental studies have confirmed that mechanical strain can effectively control the electronic structure and transport response of carbon-based materials. Particularly for graphene, which is a gapless material, the use of mechanical forces as control parameters can establish important strategies for envisioning band-gap engineering and the development of logical molecular switching devices.⁹⁻¹⁴

Miniaturization strategies for electronic devices have encouraged intense research focusing on the physical properties of low-dimensional systems, in special, single covalent carbon chains.¹⁵ The structural dynamics of carbon atomic chains such as formation, migration, and breakage have been addressed by several experimental methods. For instance, stable and rigid carbon atomic chains have been experimentally realized by removing rows of carbon atoms from graphene¹⁶ and multi-walled carbon nanotubes¹⁷ via energetic electron irradiation techniques.

The controlled way of producing such rigid linear chains can dictate the design of novel building-block components for electronic devices at the molecular scale. Carbon atomic chains bridging graphene-based structures have been suggested to regulate the switching operation mechanisms of nonvolatile memory elements where pulse electric gates trigger the formation and breaking of the chains.¹⁸ The formation of carbon chains can rule the main onset of conductance quantization behavior observed just before junction breakdown as well

as the closing of the conduction channel after the rupture. The understanding of the formation of carbon atomic chains in mechanically modified graphene-based materials therefore is an important issue, either to achieve the ultimate basic component of molecular devices or to understand novel memory concepts based on graphene atomic switches.

In this paper, we study the electronic and structural changes of graphene nanoribbons (GNRs) under mechanical stress until the GNRs break completely. We adopted an density-functional-based tight-binding molecular dynamics (DFTB-MD) approach to search for favorable physical conditions that can induce optimal switching features of strained nanoribbon devices. Large structural modifications and defects as well as linear carbon chains are formed immediately before breakage. These results reinforce the proposed interpretation published in Ref. 18 concerning the possible creation of ultimate single carbon-chain-based conducting channels.

Molecular dynamics results. We performed molecular dynamics (MD) simulations using DFTB-MD.^{19,20} DFTB formalism consists of a second-order expansion of the Khon-Sham total energy density functional theory (DFT) functional with respect to charge density fluctuations. The MD ingredient embedded in the DFTB method allows us to calculate the force calculation on the fly as the system dynamically transforms. The equation of motion for the atoms during the simulations has been integrated using the standard velocity Verlet method with a fixed time step of 0.25 fs, and an Andersen thermostat was applied to keep the system at room temperature. Mechanical stretching was done by pulling away the atoms located on the right side of the supercell at incremental values of 0.009 Å while keeping the left side fixed. The equivalent mechanical energy resulting from the stretching is defined as $E_M = -\Delta\vec{L} \cdot \vec{F}$, with \vec{F} being the external force and $\Delta L = L - L_0$, where L and L_0 are the deformed and initial equilibrium lattice constant parameters along the axial direction, respectively. The strain is given by $\Delta L/L_0$.

An extensive study about the interplay between mechanical and electrical properties of several GNRs was carried out

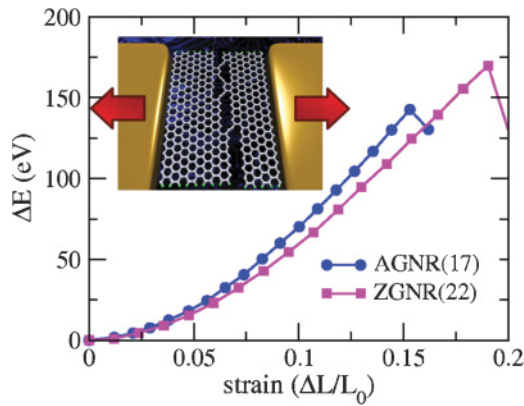


FIG. 1. (Color online) Dependence of relative energy on the strain for GNRs with different widths and edge chiralities: the curve with circle symbols (blue) corresponds to an AGNR (17) and the curve with square symbols (magenta) corresponds to a ZGNR (22). Inset: Ball-and-stick representation of a GNR under strain. The arrows (red) point to the direction where the mechanical forces are applied.

considering both zigzag [ZGNR (N)] and armchair [AGNR (N)] edge geometries. N denotes the number of carbon dimers distributed along its width. The dependences of the total energy with respect to strain for two representative GNR samples are shown in Fig. 1. The total energy curves exhibit a quadratic behavior as a function of strain. Our results demonstrate excellent agreement with previous first principal calculations performed by other groups.^{10,21} Mechanical constants within a true elastic regime of several GNR configurations were determined, such as force constants $\kappa = (180\text{--}200)$ N/m and in-plane stiffness $C = (290\text{--}300)$ N/m. We can also identify the yield point that delimits the threshold where the ribbons begin to deform plastically. Both A- and ZGNR structures can be elastically deformed prior to the strain value of 13%. Beyond this critical point, the samples can suffer some permanent deformation or even split completely. For instance, AGNR (17) breaks at 15% strain, and ZGNR (22) fractures at higher values, around 20%. This indicates that ZGNRs accumulate more potential energy than AGNRs at the breaking point.

The atomic arrangement of the ribbons as the mechanical strain increases can be seen on the lower panels of Figs. 2 and 3 for AGNRs and ZGNRs, respectively. Our results clearly point to the formation of small carbon atomic chains as strain is loaded on the systems. In fact, AGNRs are more prone to create carbon chains than ZGNRs. Several MD simulations show that most of the ZGNRs structures do not reveal a one-dimensional (1D) carbon bridge but simply a discontinuous breakage. In contrast, strained AGNR configurations seem to be more propitious for the formation of atomic chains where not only one link can emerge from the stretching but also two or even three along the lateral size. The wider the AGNR is, more carbon chains can be observed; for instance, seven 1D carbon bridges were found for AGNR (30). This can be explained by the fact that the accumulated potential energy at the breakage can be converted into kinetic energy. In this sense, the higher potential energy of ZGNRs in comparison to the AGNRs can be transformed into a more intense dynamic response of the atoms, which leads to an abrupt breakage. These

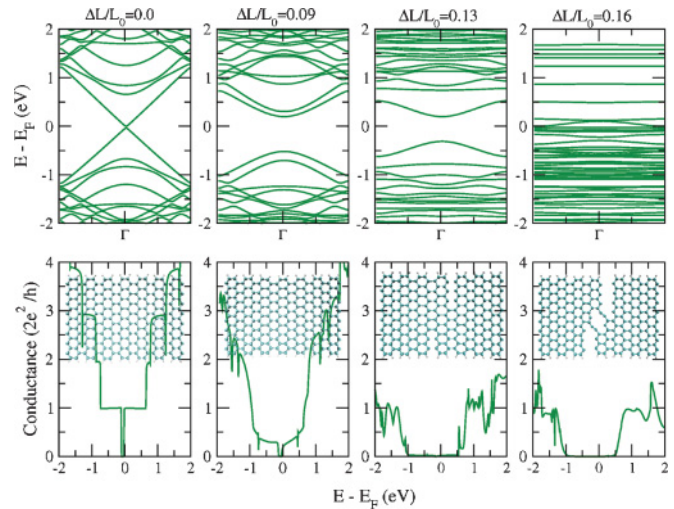


FIG. 2. (Color online) Top and bottom panels display band structures and conductance vs Fermi energy, respectively, for different strain intensities. Insets: atomic arrangements of relaxed ($\Delta L/L_0 = 0.0$) and stretched ($\Delta L/L_0 \neq 0.0$) AGNR (17) obtained from MD simulations.

results are in agreement with previous calculations performed for stretching carbon nanotubes following a DFTB approach as well.¹⁹

Another important issue to stress here is the main role played by Peierls distortion on the formation of the linear chains.²² One knows that isolated infinite sp carbon species can exhibit alternating single and triple bonds, called polyynes, or identical double bonds, called cumulenes.^{10,11} Our calculations for a wide variety of GNR geometries show that both cumulene and polyyne structures can be generated during the stretching process. An intriguing example was found for an AGNR (9), in which both allotropic forms of chains were observed before its breakdown.

Electronic and transport properties. Following the atomic structural investigation of strained ribbons, we explore how such structural deformations induced by stretching are actually connected to their conduction properties. This can be done analyzing their electronic structure and transport response with respect to the strain intensity. The band structures and electronic transmission of the systems are determined using the DFTB method within Green's function formalism following Landauer's approach. The results are given in Figs. 2 and 3 for an AGNR (17) and a ZGNR (22), respectively. For the band-structure calculations, the whole scattering region that will be submitted to strain composes our supercell, and it will be treated by imposing periodic boundary conditions. In the transport calculations, the systems are modeled with open-boundary conditions where left and right electrodes are considered as semi-infinite graphene ribbons transparently connected to a central scattering region.

First, in Fig. 2 we present the energy band relations (top panels) and quantum conductance curves (bottom panels) obtained for an AGNR (17) under different strains. The corresponding deformed atomic configurations are displayed in the insets. Remarkable changes in the electronic structure of a mechanically modified AGNR-based junction can be observed. The characteristic steplike profiles of the electronic

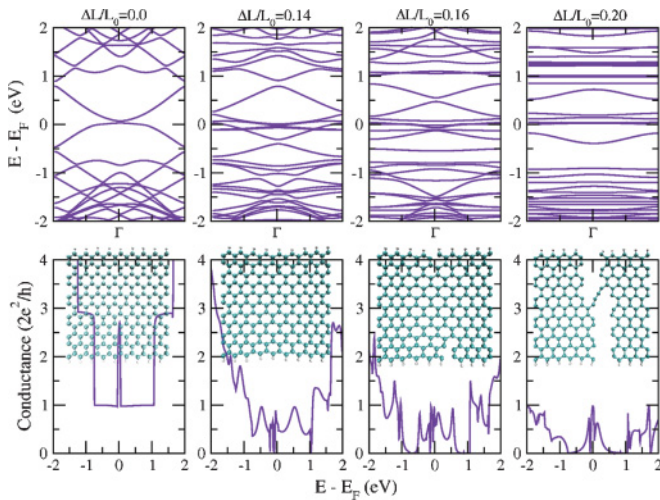


FIG. 3. (Color online) Top and bottom panels display band structures and conductance vs Fermi energy, respectively, for different strain intensities. Insets: atomic arrangements of relaxed ($\Delta L/L_0 = 0.0$) and stretched ($\Delta L/L_0 \neq 0.0$) ZGNR (22) obtained from MD simulations.

transmission of ideal GNRs are smoothed out by the ensemble averaging taken randomly from MD simulations. These results confirm that mechanical stretching can cause a significant decrease in the conductance in a wide energy range around the charge neutrality point (CNP). Previous works following the static equilibrium approximation found that uniaxial forces an efficient control parameter for pristine nanoribbons,¹³ The symmetry of perfect nanoribbons is represented by the space point group D_{2h} and, within a static approach, such states remain invariant regardless of the amount of mechanical strain.

Metal-semiconductor transition can be induced in AGNRs by strain due to the rearrangement of the electronic orbitals whenever the bonds are stretched. This can be explained by the fact that mechanical forces deform the graphene's Brillouin zone in relation to the allowed confined states of the ribbon. Physical effects are revealed as the system is dynamically treated because D_{2h} symmetry is completely lost as a result of the formation of defects. This reflects in an energy gap opening, which can reach a maximum value of $E_g = 1.7$ eV when $\Delta L/L_0 = 0.13$. Through the conductance results, it is possible to observe the reduction of the electronic transmission around the CNP. At approximately $\Delta L/L_0 = 0.11$ (not shown), the single quantum channel at low energy is completely blocked. At higher energy ranges, the majority of transmission channels are also quenched with the enhancement of mechanical strain as a consequence of the flatness of the band states.

The same analysis is presented for a ZGNR (22) in Fig. 3. As one knows, the electronic structure of pristine ZGNRs is characterized by the presence of twofold degenerate edge states at the Fermi energy, which decay exponentially into the center of the ribbon. As we already learned from our previous static calculations, the energy dispersion of ZGNRs almost does not suffer significant strain-induced modifications.¹³ A reminiscence of such robustness close to the CNP is once more observed. While increasing the strain intensity, the bands tend to flatten, but the degeneracy at the Γ point is not split. In the vicinity of CNP, the conductance maintains a constant value

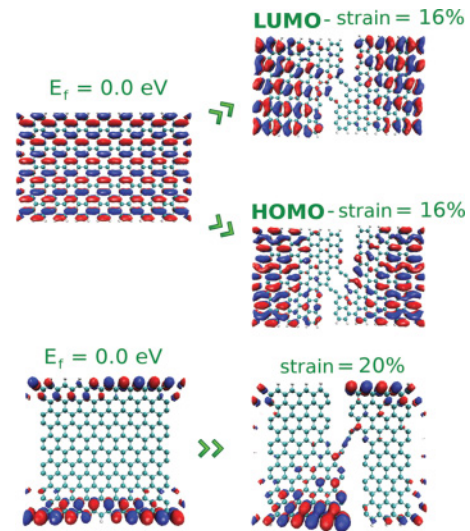


FIG. 4. (Color online). Wave functions calculated at the Γ point for AGNR (17) (upper panels) and ZGNR (22) (bottom panels) for relaxed structures and structures under strain ($\Delta L/L_0 = 16\%$ and 20% , respectively). The selected energy levels are in the proximity of the CNP for both armchair and zigzag geometries and the highest occupied molecular orbital (HOMO) and the lowest unoccupied molecular orbital (LUMO) states for strained AGNR (17). Red (gray) and blue (dark gray) colors correspond to positive and negative coefficients, respectively.

of $G = 2e^2/h$. This robustness under uniaxial stretching again can be explained by the picture of Brillouin zone deformation. When the ribbon is under uniaxial stress, the quantum state at CNP follows a trajectory in the Brillouin zone that never deviates from the $\Gamma - K$ line, and the degeneracy of the flat bands cannot be lifted. On the other hand, our current dynamic simulations show that the overall electronic structure of zigzag geometries is rather sensible to mechanical forces that could not be predicted via static approximation.

To complete such a transport analysis, we address the behavior of spatial conduction channels for the charge carriers along the scattering region. All the quantum mechanical information of the electronic structures is visualized through molecular orbital pictures that are depicted in Fig. 4, which shows the wave functions calculated at the Γ point for different energies when the ribbons AGNR (17) and ZGNR (22) are under relaxed and strained conditions ($\Delta L/L_0 = 16\%$ and 20% , respectively). The characteristic delocalized behavior of the states for a relaxed AGNR (17) is transformed into a rather localized profile, especially on the region near the carbon chains. The separation of the structure is not symmetric with respect to its center, and this leads to irregular interference patterns of the electronic states. The states from left and right electrodes do not superimpose through the carbon chains. This suggests that the presence of defects generated on the strained junction does not favor the electronic transport in AGNR geometries. We then expect that AGNRs can display promising switching features in the true elastic regime where the structure can be reversibly deformed between ON and OFF states. Binary ON/OFF states cannot be selected when the system is near breakage. The opposite can be obtained for ZGNR (22), which depicts an open conducting channel even at strains close to

the breakdown. We could conclude that zigzag ribbons are not good switches, but in reality, they pose a scenario that is similar to the switching device proposed by Standley *et al.*¹⁸ The ON state is stable during the whole stretching process until the moment that this channel can be conducted to an OFF condition after the rupture. It is also interesting to notice that the electronic propagation is mostly done along the edges. The amplitude of the wave functions has pronounced contributions along the ribbon's edge. Our study highlights the crucial role played by geometrical aspects on the transport properties of GNRs, in particular, the shape of their edges.

Conclusion. Systematic research about structural, electronic, and transport properties on GNRs under uniaxial stretching has been reported. For both initial edge geometry of the considered ribbon (zigzag or armchair), carbon chains are formed by bridging left and right graphene segments, although this is less frequent in ZGNRs. We investigated the main

physical mechanisms that can favor the use of graphene-based junctions in ultrasmall molecular switching devices. For armchair geometries, the systems can be reversibly tuned between metal and semiconducting characters as a function of strain. Zigzag ribbons are promising conditions for strain-induced switching near breakage because of the robustness of the conductance near the CNP. These studies show fundamental issues related to the experimental realization made by Standley *et al.*¹⁸ in which the operation mechanism of graphene-based switches is ruled by the formation and breakage of carbon chains bridging separated graphene flakes.

Acknowledgments. This work is supported by the European Union and the Freistaat Sachsen (Project No. 13857/2379), the NANOSIM-GRAPHENE Project (ANR-09-NANO-016-01) of ANR/P3N2009, and the Alexander von Humboldt Foundation.

*ezgierdo@gmail.com

- ¹A. V. Krasheninnikov and F. Banhart, *Nat. Mat.* **6**, 723 (2007); A. V. Krasheninnikov and K. Nordlund, *J. Appl. Phys.* **107**, 071301 (2010); E. Holmström, L. Toikka, A. V. Krasheninnikov, and K. Nordlund, *Phys. Rev. B* **82**, 045420 (2010).
- ²M. T. Lusk, D. T. Wu, and L. D. Carr, *Phys. Rev. B* **81**, 155444 (2010).
- ³J. C. Charlier, X. Blase, and S. Roche, *Rev. Mod. Phys.* **79**, 677 (2007).
- ⁴A. H. Castro Neto *et al.*, *Rev. Mod. Phys.* **81**, 109 (2009).
- ⁵A. Cresti, N. Nemeč, B. Biel, G. Niebler, F. Triozon, G. Cuniberti, and S. Roche, *Nano Res.* **1**, 361 (2008).
- ⁶F. Xia, D. B. Farmer, Y.-M. Lin, and P. Avouris, *Nano Lett.* **10**, 715 (2010).
- ⁷L. G. De Arco, Y. Zhang, C. W. Schlenker, K. Ryu, M. E. Thompson, and C. Zhou, *ACS Nano* **4**, 2865 (2010).
- ⁸A. K. Hüttel *et al.*, *Nano Lett.* **9**, 2547 (2009).
- ⁹V. M. Pereira and A. H. Castro Neto, *Phys. Rev. Lett.* **103**, 046801 (2009); V. M. Pereira, A. H. Castro Neto, and N. M. R. Peres, *Phys. Rev. B* **80**, 045401 (2009); O. Hod and G. E. Scuseria, *Nano Lett.* **9**, 2619 (2009).
- ¹⁰M. Topsakal and S. Ciraci, *Phys. Rev. B* **81**, 024107 (2010); M. Topsakal, V. M. K. Bagci, and S. Ciraci, *ibid.* **81**, 205437 (2010).
- ¹¹E. Hobi, R. B. Pontes, A. Fazzio, and A. J. R. da Silva, *Phys. Rev. B* **81**, 201406 (2010).
- ¹²Y. Wang, Z.-Z. Lin, W. Zhang, J. Zhuang, and X.-J. Ning, *Phys. Rev. B* **80**, 233403 (2009).
- ¹³M. Poetschke, C. G. Rocha, L. E. F. Foa Torres, S. Roche, and G. Cuniberti, *Phys. Rev. B* **81**, 193404 (2010); Y. Li *et al.*, *Nano Res.* **3**, 545 (2010).
- ¹⁴T. M. G. Mohiuddin, A. Lombardo, R. R. Nair, A. Bonetti, G. Savini, R. Jalil, N. Bonini, D. M. Basko, C. Galiotis, N. Marzari, K. S. Novoselov, A. K. Geim, and A. C. Ferrari, *Phys. Rev. B* **79**, 205433 (2009).
- ¹⁵Z. Zanolli, G. Onida, and J.-C. Charlier, *ACS Nano* **4**, 5174 (2010); W. Chen, A. V. Andreev, and G. F. Bertsch, *Phys. Rev. B* **80**, 085410 (2009).
- ¹⁶C. Jin, H. Lan, L. Peng, K. Suenaga, and S. Iijima, *Phys. Rev. Lett.* **102**, 205501 (2009).
- ¹⁷F. Borner *et al.*, *Phys. Rev. B* **81**, 085439 (2010).
- ¹⁸B. Standley, W. Bao, H. Zhang, J. Bruck, and C. N. Lau, and M. Bockrath, *Nano Lett.* **8**, 3345 (2008); J. Yao, L. Zhong, Z. Zhang, T. He, Z. Jin, P. J. Wheeler, D. Natelson, and J. M. Tour, *Small* **5**, 2910 (2009).
- ¹⁹D. Porezag, T. Frauenheim, T. Kohler, G. Seifert, and R. Kaschner, *Phys. Rev. B* **51**, 12947 (1995); V. V. Ivanovskaya *et al.*, *Small* **1**, 399 (2005).
- ²⁰G. Seifert, D. Porezag, and T. Frauenheim, *Int. J. Quantum Chem.* **58**, 185 (1996).
- ²¹D. Sen, K. S. Novoselov, P. M. Reis, and M. J. Buehler, *Small* **6**, 1108 (2010).
- ²²A. Karphen, *J. Phys. C* **12**, 3227 (1979).